Robotica: (2020) volume 38, pp. 427–441. © Cambridge University Press 2019
doi:10.1017/S0263574719000742

Theoretical Study of Global Scale Analysis Method for Agile Bionic Leg Mechanism

Hongbin Zang†‡*, Dengfeng Zhao‡ and Lianguan Shen†

† *Department of Precision Machinery and Precision Instrumentation, University of Science and Technology of China, Hefei 230027, China*
‡ *Key Laboratory of Testing Technology for Manufacturing Process of Ministry of Education, Southwest University of Science and Technology, Mianyang 621010, China*

(Accepted April 25, 2019. First published online: June 19, 2019)

SUMMARY
Agile bionic leg mechanism (ABLM) has attracted more and more attention in the development of jumping robots and high-speed running robots. However, theoretical study of the global structure for motility characteristics and its evolution is few. By using the modern mathematical tools such as singular theory, geometric topology, and group theory, a global scale analysis method for kinematic performance of mechanisms is proposed. Taking 6-bar with two rings mechanism as an example, a detailed analysis process is studied. The 6-bar ABLM designed by this theory is verified by virtual prototype simulation experiment. The global scale analysis of 4-bar linkage is also carried out by using this method, and the result is compared with the "Grashof criterion" to verify the correctness of this method. It provides a general theory and method for innovative design and global scale analysis of ABLM.

KEYWORDS: Agile bionic leg mechanism; Theoretical study; Global scale analysis method; Verification; General theory and method.

1. Introduction

In recent years, more attentions are drawn to high-speed running bionic leg and jumping bionic leg, because they are the most important topics in the field of legged robots which require strict constraints on structural design, control, and state perception. Generally speaking, two methods contribute to the high-speed running or high-jumping performance of robot.

The traditional way is the utility of high-power actuators. Robots like "LittleDog," "HYQ," "Baby Elephant," and "MBBOT" have been developed in this way, of which "BigDog" is the most representative one. The LittleDog robot has 12 active joints that are driven by electric motors.[1] Each leg of the HyQ has three active revolute joints which are powered by both hydraulic and electric actuators.[2,3] The Baby Elephant uses a 10 kW DC motor to drive the hydraulic system.[4] The MBBOT has six Degree of Freedom (DOF) on torso and five DOF on each leg.[5] The BigDog uses four articulated links and three active revolute joints that are powered by hydraulic cylinders on each leg.[6,7] However, driving actuators of these robots are mounted on the leg joints that require clockwise and anticlockwise rotation periodically when the leg swings back and forth, which reduces the working efficiency of the actuators.[8]

Another new effective way is to change the leg morphologies and the linkage design of the leg mechanism is the key point. Driving motors are mounted directly on the body, which can transform the continuous rotation of the motors to the swinging back and forth of the legs. Then, the mass

*Corresponding author. E-mail: zanghongb@163.com

https://doi.org/10.1017/S0263574719000742 Published online by Cambridge University Press

and rotating inertia of the legs decrease. So, we call this kind of legs as agile bionic leg mechanism (ABLM). The advantages of ABLM in high-speed running[9,10] and high-jumping[11–14] have been verified by many studies. Some representative research results are as follows: "Salto," "Cat-inspired robot," "MIT Cheetah," and "Planar Elliptical Runner (PER)." Salto robot uses a planar 8-bar revolute linkage to encode an mechanical advantage (MA) profile for enabling power modulation.[15] 9-bar linkage is used for Cat-inspired robot to drive the leg with one actuator.[16] The MIT Cheetah uses 4-bar revolute linkage to achieve a cost of transport that matches running animals in nature.[17–19] PER is the first bipedal bionic robot in the world which tries to not rely on sensors or computers to achieve high-speed running and keep its own balance.[20] Compared with the traditional way,[21–26] they have the characteristics of ingenious mechanism,[27] small moment of inertia,[28] light weight,[29] high efficiency,[30] and simple controlling.[31–33]

Although ABLMs have been studied so much, they still adopt the traditional theoretical analysis method based on vector loop equations or D-H parameter method, without giving innovative design and analysis theory. Theoretical study of the global scale analysis method (GSAM) for ABLM is few. It cannot provide a general theory and method for global scale analysis of ABLM.

The study of GSAM can be traced back to 19th century, in which "Grashof criterion" is the most well known. The global characteristics of 4-bar mechanisms are clearly revealed through simple Grashof inequality. Since then, scholars have tried to extend it to analyze other complicated mechanisms. However, the study on the relations between the global motion characteristics and the singularity of mechanisms is few. Gao et al.[34] introduced the concept of solution space to the mechanisms evolution analysis, and the workspace atlas of parallel planar manipulators was obtained. Zhao et al.[35,36] used the convex hull division method to explore the classification method of single-loop planar and spherical mechanisms. Our research focuses on the theoretical study of GSAM for ABLM.

In this paper, a GSAM which is based on strict mathematical theory is put forward by using modern mathematical tools such as singular theory, geometric topology, and group theory. The global distribution characteristics of the motion performance and its evolution with the global scale are studied. This method will solve too many intuition judgment problems in the scale design of ABLM, and greatly expand the vision of the configuration design and comprehensive analysis of ABLM. It provides a rich configuration and scientific theoretical analysis method for the design of ABLM. It also provides a general theory and method for innovative design and global scale analysis of ABLM.

The rest of this paper is organized as follows: Section 1 describes mechanism characteristics of ABLM. In section 2, constraint equation and singularity analysis of mechanism are given. Symmetry and the division of basic regions are shown in section 3. Taking 6-bar with two rings mechanism as an example, a detailed analysis process is studied. Furthermore, the 6-bar ABLM designed by GSAM is verified by virtual prototype simulation experiment in section 4. The global scale analysis of 4-bar linkage is also carried out by using this method, and the result is compared with the "Grashof criterion" to verify the correctness of this method in section 5. The conclusion and possible future research are given in section 6.

2. Mechanism Characteristics of Agile Bionic Legs

According to the motion characteristics of the ABLM, the mechanism characteristics are as follows:

(1) A linkage mechanism driven by a single DOF. The planar linkage mechanism is used for dexterity design. The active drive of the whole bionic leg mechanism is single DOF, so that the coordinated control of the leg motion can be realized without excessive dependence on the sensor system and the complex control algorithm.
(2) Leg mass ratio (leg mass to whole robot mass ratio) is small. The driving element is installed on the body of the robot to reduce the mass ratio of the leg and reduce the moment of inertia at the high speed of the leg, so that it has the characteristics of dexterity, agility, and efficiency.
(3) Continuous drive. The driving elements do not need positive, reverse, commutation, acceleration, and deceleration control, so that the bionic leg joints can be coordinated, and bionic movement and whole leg stride motion can be realized.

According to the motion characteristics of the agile bionic leg and the structural features of the mechanism and the existing mechanism design theory, it is not difficult to design the innovative

https://doi.org/10.1017/S0263574719000742 Published online by Cambridge University Press

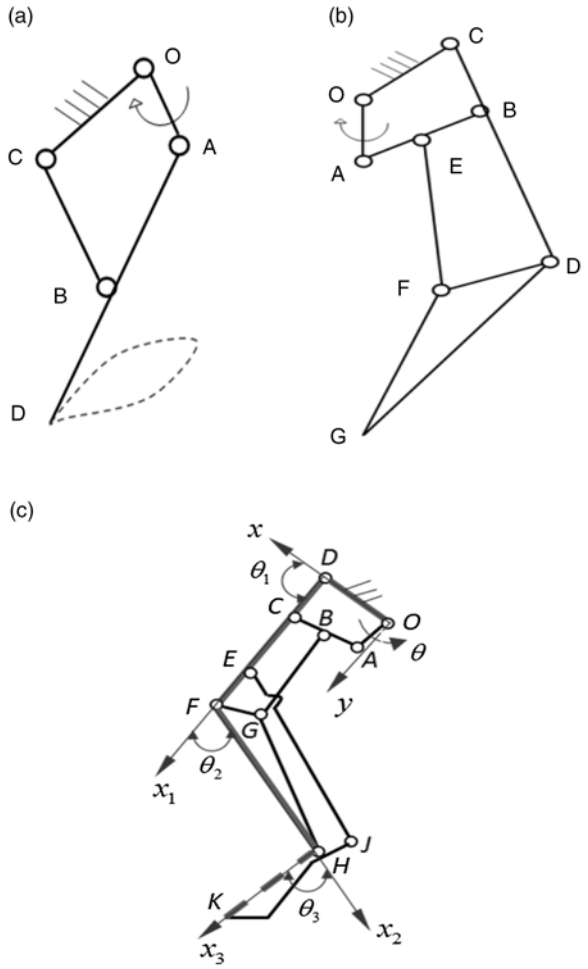


Fig. 1. Agile bionic leg mechanism (ABLM). (a) The 4-bar configurations, which is a planar single ring mechanism. (b) The 6-bar configurations, which is a planar double-ring mechanism. (c) The 8-bar configurations, which is a planar multi-ring mechanism.

design of the ABLM. The typical 4-bar, 6-bar, and 8-bar configurations are shown in Fig. 1(a)–(c), which belong to planar single ring or multi-ring linkage mechanism.

The distribution of the motion and performance parameters of the mechanism will evolve with the changes in the scale of the component. This evolution process may be gradually evolved and also may be mutated. It is this kind of mutation that produces the scale classification of the mechanism. The overall situation of motion and performance parameters along with mechanism size evolution is very important for the design of agile bionic legs.

Therefore, based on the topological structure mutation of the mechanism solution space, the scale classification method of complex mechanism is studied; based on the mechanism of the spatial singular partition, the global structure and distribution characteristics of the mechanism are studied; based on the mutation of solution space division, the morphological evolution of the performance distribution of the mechanism is studied.

3. Constraint Equation and Singularity Analysis of Mechanism

The mechanism can be regarded as a nonlinear geometric constraint equation which is defined on the space variable of the motion parameters and the spatial variables of the structural parameters when the mechanism analysis and the comprehensive problems are viewed from the point of mathematics. All the characteristics of mechanism performance depend on the characteristics of constrained equations and are completely reflected in the solution space.

The 6-bar ABLM shown in Fig. 1(b) is essentially a planar double ring as shown in Fig. 2. Its motion space parameters are $u = (\theta_1, ..., \theta_6)$, structural space parameters are $v = (l_1, ..., l_6, l'_3, l'_4)$,

https://doi.org/10.1017/S0263574719000742 Published online by Cambridge University Press

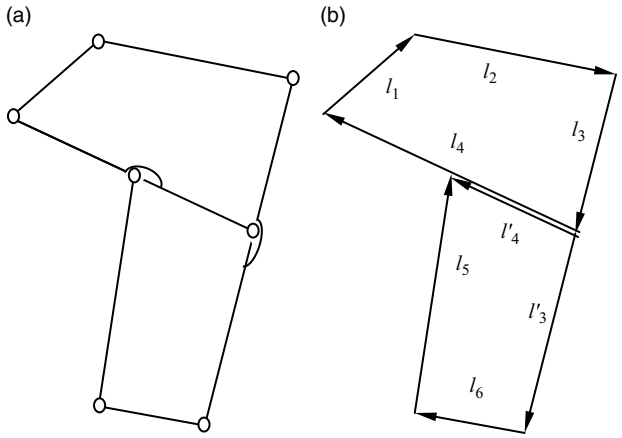


Fig. 2. The 6-bar planar double-ring mechanism. (a) Diagram of 6-bar planar double-ring mechanism. (b) Vector relation diagram of 6-bar planar double-ring mechanism.

and θ_i represent the angles between the vector l_i and the horizontal axis. The constraint equation of mechanism is the double closed ring and its condition is Eq. (1).

$$\begin{cases} l_1 \cos\theta_1 + l_2 \cos\theta_2 + l_3 \cos\theta_3 + l_4 \cos\theta_4 = 0 \\ l_1 \sin\theta_1 + l_2 \sin\theta_2 + l_3 \sin\theta_3 + l_4 \sin\theta_4 = 0 \\ l'_3 \cos\theta_3 + l'_4 \cos\theta_4 + l_5 \cos\theta_5 + l_6 \cos\theta_6 = 0 \\ l'_3 \sin\theta_3 - l'_4 \sin\theta_4 + l_5 \sin\theta_5 + l_6 \sin\theta_6 = 0 \end{cases} \tag{1}$$

The nondegenerate singular problem is determined by the Jacobi matrix J of the constraint equation on the moving space parameters.

$$J = \begin{bmatrix} -l_1 \sin\theta_1 & -l_2 \sin\theta_2 & -l_3 \sin\theta_3 & -l_4 \sin\theta_4 & 0 & 0 \\ l_1 \cos\theta_1 & l_2 \cos\theta_2 & l_3 \cos\theta_3 & l_4 \cos\theta_4 & 0 & 0 \\ 0 & 0 & -l'_3 \sin\theta_3 & -l'_4 \sin\theta_4 & -l_5 \sin\theta_5 & -l_6 \sin\theta_6 \\ & & l'_3 \cos\theta_3 & l'_4 \cos\theta_4 & l_5 \cos\theta_5 & l_6 \cos\theta_6 \end{bmatrix} \tag{2}$$

When the Jacobi matrix J is a reduced rank matrix, the topological mutation of the solution space occurs, and the overall distribution characteristics of various performance parameters of the mechanism also occur abrupt, which constitutes the basic condition for the classification of the mechanism. At this time, the determinant of 4×4 matrices which is extracted from four columns of J is "0," and the lower rank conditions are derived as follows:

$$\begin{cases} \sin(\theta_i - \theta_j) = 0 & i, j \in \{1, 2, 3, 4\} \\ \sin(\theta_i - \theta_j) = 0 & i, j \in \{3, 4, 5, 6\} \end{cases} \tag{3}$$

The first line of this formula contains six conditions. They are the relations between "and." When the six conditions satisfy $\theta_1 = \theta_2 = \theta_3 = \theta_4$ at the same time, the mechanism solution space mutation, at this time the components (l_1, l_2, l_3, l_4) are the same direction or the reverse collinear. The second way also contains six conditions to satisfy $\theta_5 = \theta_6 = \theta_3 = \theta_4$, when components (l'_3, l'_4, l_5, l_6) are in the same direction or reverse collinear. The two sets of conditions are the "or" relationship. That is to say that any groups satisfy this condition. Then the space of solution is mutated. The two sets of conditions are substituted into the constraint equations and the motion parameters are eliminated, then the solution space of the two groups of structural spaces is obtained as follows.

$$\begin{cases} \pm l_1 \pm l_2 \pm l_3 \pm l_4 = 0 \\ \pm l'_3 \pm l'_4 \pm l_5 \pm l_6 = 0 \end{cases} \tag{4}$$

When the structural parameters span these two sets of conditions and confirm that they satisfy the collinear condition of the components, the topology structure of the solution space is abrupt. There are 16 conditions for the two sets of mutation conditions, and they will be used to classify the structural space to achieve mechanism scale classification.

https://doi.org/10.1017/S0263574719000742 Published online by Cambridge University Press

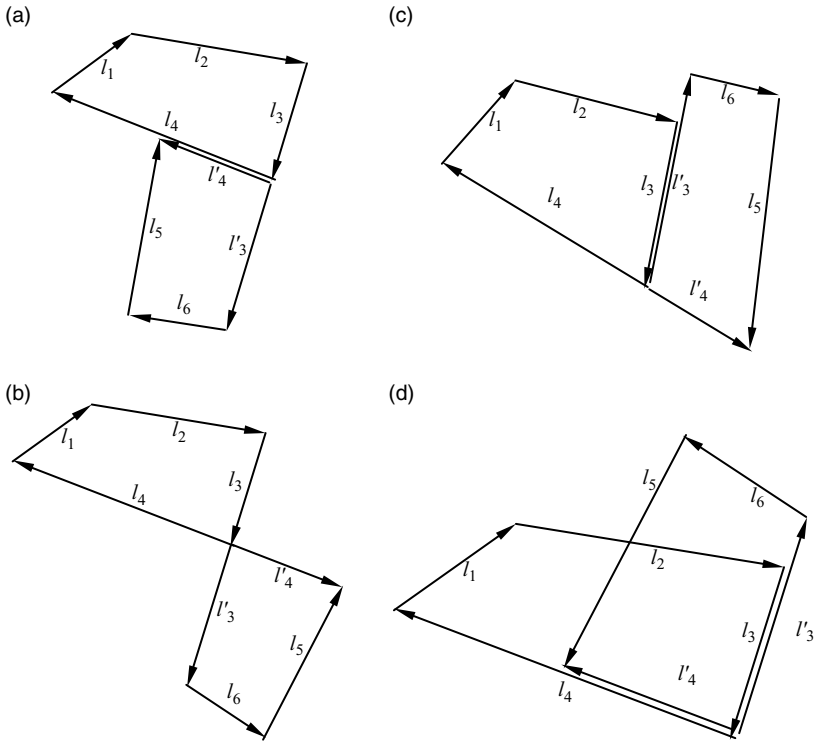


Fig. 3. Simultaneous inversion and mechanism classification of (l'_3, l'_4). (a) and (c) The first kind of mechanism; (b) and (d) the second kind of mechanism.

4. Symmetry and the Division of Basic Regions

A nonsingular transformation F is performed for the motion parameters and structural parameters of the mechanism. There is a nonsingular transformation F' for the constraint equation, which makes the form of the constraint equation completely unchanged. Then, F is the symmetric transformation of the mechanism and the F' is the dual transformation of F. All symmetric transformations of a mechanism constitute a transformation group, which reflect all symmetrical properties of the mechanism. Using these symmetric properties, we can simplify the partition of structural space and eliminate the classification of false mechanisms with symmetric properties. The mechanism constraint Eq. (1) has the following symmetry.

(1) Inverse symmetry of structural parameters

In the structural parameters (l_1, l_2, l_5, l_6), any structural parameter l_i changes to $-l_i$ and θ_i to $\theta_i + \pi$, and the constraint Eq. (1) remains unchanged (constant same transformation). According to this symmetry, we only need to analyze the part of $l_i > 0$. A parameter reduces 1/2, and the structural space partition area of four structural parameters is reduced to the original 1/16. We only need to analyze the first quadrant of the four-dimensional (l_1, l_2, l_5, l_6) parameter subspace.

The structural parameters l_3 and l'_3 (or l_4 and l'_4) change contrarily simultaneously, i.e. increasing the corresponding θ_3 (or θ_4) with π. The constraint in Eq. (1) keeps unchanged. This symmetry brings an advantage that only the part of $l_3 > 0$ (and $l_4 > 0$) is analyzed. The analysis area is further reduced to 1/4 of the original area.

The (l'_4, l'_3) becomes $(-l'_4, -l'_3)$ at the same time, and the motion parameters (θ_5, θ_6) plus π, such as the transformation between the Fig. 3(a), (c) and (b), (d), and then the dual transformation is executed, that is, the third and fourth lines of the constraint Eq. (1) is multiplied by "–1," and the equation is restored to the same. This symmetry only analyzes the $l'_3 > 0$ part, which will also reduce the scope of the analysis by half.

The analysis range of l'_4 is still all real range. In order to analyze the mechanism of $l'_4 < 0$ as another kind of mechanism, the mechanism is divided into two categories. As shown in Fig. 3, the (a) and (c) are classified as one class, and (b) and (d) are classified as another class, and the length of each bar is more than "0."

https://doi.org/10.1017/S0263574719000742 Published online by Cambridge University Press

In Fig. 3(a) and (c), the corresponding $(\theta_1, \theta_2, \theta_3, \theta_4)$ are the same, but the corresponding (θ_5, θ_6) are different with π. In Fig. 3(b) and (d), the corresponding $(\theta_1, \theta_2, \theta_3, \theta_4)$ are also the same and the corresponding (θ_5, θ_6) are also different with π. The solution of the motion parameters in the group of Fig. 3(a) and (c) are different from that in the group of Fig. 3(b) and (d). Therefore, in the following analysis, we call the mechanism in Fig. 3(a) and (c) as the first kind of mechanism and the mechanism in Fig. 3(b) and (d) as the second kind of mechanism.

(2) Projective symmetry

The structural parameters (l_1, l_2, l_3, l_4) are multiplied by an arbitrary nonzero real number λ_1, and the first and second formulae of the constraint Eq. (1) are divided by λ_1 at the same time; the constraint equation is kept unchanged. For the convenience of analysis, constraint condition $l_1 + l_2 + l_3 + l_4 = 1$ is introduced. The structural parameters (l_3, l_4, l_5, l_6) are multiplied by an arbitrary nonzero real number λ_2, and the first and second formulae of the constraint Eq. (1) are divided by λ_2 at the same time. The constraint equation is kept unchanged and the constraint condition $l'_3 + l'_4 + l_5 + l_6 = 1$ is introduced. The introduction of these two constraints will reduce the dimension of the structural space from eight dimensions to six dimensions.

(3) The symmetry of replacement

When the structure parameters (l_1, l_2) and motion parameters (θ_1, θ_2) are exchanged at the same time, Eq. (1) is invariable. So, we only analyze the $l_1 > l_2$ part. Similarly, when the structure parameters (l_5, l_6) and motion parameters (θ_5, θ_6) are exchanged at the same time, Eq. (1) is invariable. So, we only analyze the $l_5 > l_6$ part.

When the structural parameters (l_3, l_4) and motion parameters (θ_3, θ_4) are exchanged at the same time, the first and the second row in Eq. (1) are invariant. θ_5 is replaced by $\theta_3 + \theta_4 - \theta_5$ and θ_6 is replaced by $\theta_3 + \theta_4 - \theta_6$. The dual transformation of this transformation is to let the third and fourth row in Eq. (1) multiply a rotation transformation matrix $[\cos(\theta_3 + \theta_4)\sin(\theta_3 + \theta_4); \sin(\theta_3 + \theta_4)\cos(\theta_3 + \theta_4)]$. That is to say each angle is rotated by $-(\theta_3 + \theta_4)$. So, we can just analyze the $l_3 > l_4$ part.

In the same way, when the structural parameters (l'_3, l'_4) and motion parameters (θ_3, θ_4) are exchanged at the same time, the third and the fourth row in Eq. (1) are invariant. θ_1 is replaced by $\theta_3 + \theta_4 - \theta_1$ and θ_2 is replaced by $\theta_3 + \theta_4 - \theta_2$. The dual transformation of this transformation is to let the first and second row in Eq. (1) multiply a rotation transformation matrix $[\cos(\theta_3 + \theta_4)\sin(\theta_3 + \theta_4); \sin(\theta_3 + \theta_4)\cos(\theta_3 + \theta_4)]$. That is to say each angle is rotated by $-(\theta_3 + \theta_4)$. So, we can just analyze the $l'_3 > l'_4$ part.

When the parameters of (l_1, l_5), (l_6, l_2), (l_3, l'_3), and (l_4, l'_4) are exchanged at the same time with each other, the corresponding constraint Eq. (1) (first and third) lines and (second and fourth) rows are invariable at the same time, which means that the two rings are equal, the two 4-bar mechanisms can be discussed separately, and then the whole mechanism is analyzed by the direct product, avoiding the non-intuition of the spatial partition of the eight-dimensional structure parameters.

(4) Other symmetry

When the motion parameters $(\theta_1, \theta_2, \theta_3, \theta_4, \theta_5, \theta_6)$ are added to any angle θ_0, the constraint equation is multiplied by the rotation transformation matrix $\begin{bmatrix} \cos\theta_0 & \sin\theta_0 \\ -\sin\theta_0 & \cos\theta_0 \end{bmatrix}$, constraint equation invariance; when $(\theta_1, \theta_2, \theta_3, \theta_4, \theta_5, \theta_6)$ becomes negative at the same time, the first and third equations of constraint equations become negative and the constraint equations remain unchanged. These invariants are independent of structural parameters, so this paper is no longer to analyze. Any compound transformation of the symmetric transformation is symmetric transformation of the mechanism. All symmetric transformations constitute the transformation group of the mechanism.

5. Analysis of Global Scale Division Results

According to the above symmetry analysis, there are two reasons for the original 6-bar double-ring mechanism to be decomposed into two 4-bar single rings (l_1, l_2, l_3, l_4) and (l'_3, l'_4, l_5, l_6) mechanism's direct product: (1) according to the inversion symmetry, photographic symmetry, and permutation symmetry; and (2) parameter pairs $(l_1\theta_1, l_5\theta_5)$, $(l_6\theta_6, l_2\theta_2)$, (l_3, l'_3), and (l_4, l'_4) are swapped at the same time. This can further reduce the dimension of the analysis. Therefore, the structural spatial partition of single ring 4-bar linkage is analyzed first.

https://doi.org/10.1017/S0263574719000742 Published online by Cambridge University Press

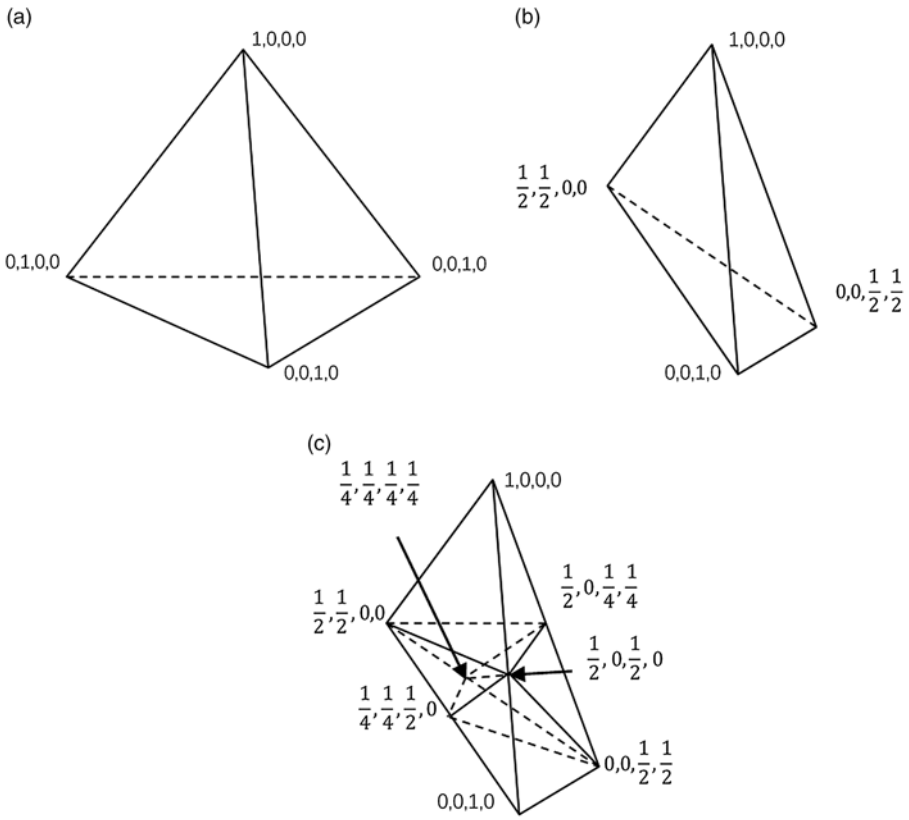


Fig. 4. Space division process of single ring (l_1, l_2, l_3, l_4) 4-bar linkage. (a) A region that satisfies first and third lines of partition conditions. (b) A region that satisfies first, second, and third lines of partition conditions. (c) Global scale partition with four partition conditions.

5.1. The result of single ring division

The structural space partition of single ring (l_1, l_2, l_3, l_4) 4-bar linkage. A total of eight partition conditions are obtained by the singular partition condition:

$$l_1 \pm l_2 \pm l_3 \pm l_4 = 0 \tag{5}$$

Obtained by symmetry analysis and division of regional conditions:

$$\begin{cases} l_1 > 0, l_2 > 0, l_3 > 0, l_4 > 0 \\ l_1 > l_2, l_3 > l_4 \\ l_1 + l_2 + l_3 + l_4 = 1 \end{cases} \tag{6}$$

The area that satisfies the division of the first and third lines of the condition (6) is the three-dimensional mono (tetrahedron) of Fig. 4(a), and the area that satisfies the three division of the region is the three-dimensional simplex as shown in Fig. 4(b).

$$\begin{cases} l_1 - l_2 - l_3 - l_4 = 0 \\ l_1 + l_2 - l_3 + l_4 = 0 \\ l_1 + l_2 - l_3 - l_4 = 0 \\ l_1 - l_2 - l_3 + l_4 = 0 \end{cases} \tag{7}$$

The division results are shown in Fig. 4. The zero-dimensional simplex, three-dimensional simplex, and main two-dimensional simplex are included in Table I.

https://doi.org/10.1017/S0263574719000742 Published online by Cambridge University Press

https://doi.org/10.1017/S0263574719000742 Published online by Cambridge University Press

Table I. Division results of structural space and corresponding mechanism properties.

Zero-dimensional simplex		Three-dimensional unit		Two-dimensional unit	
Vertex	**Coordinate**	**Vertex set**	**The properties of the mechanism**	**Vertex set**	**The properties of the mechanism**
1	(1,0,0,0)	$\sigma^3{}_0(1,3,5,7)$	No solution, the length of l_1 is longer than the sum of the rest members, and cannot form closed links	$\sigma^2{}_1(3,5,7)$	$\sigma^3{}_0$ and $\sigma^3{}_1$ worked as the transition boundary that satisfies the link length relationship $l_1 = l_2 + l_3 + l_4$
2	(0,0,1,0)	$\sigma^3{}_1(3,5,7,8)$	There is one solution, l_1 linkage is longer, mechanism without a revolving pair, and the solution is a single ring	$\sigma^2{}_2(4,5,6)$	$\sigma^3{}_0$ and $\sigma^3{}_5$ worked as the transition boundary that satisfies the link length relationship $l_3 = l_1 + l_2 + l_4$
3	(1/2,1/2,0,0)	$\sigma^3{}_2(3,5,6,8)$	There is one solution, l_1 linkage is longer, mechanism contains whole rotation motion pair, and the solution is a double ring	$\sigma^2{}_3(3,5,8)$	$\sigma^3{}_1$ and $\sigma^3{}_2$ worked as the transition boundary that satisfies the link length relationship $l_1 + l_4 = l_2 + l_3$
4	(0,0,1/2,1/2)	$\sigma^3{}_3(4,5,7,8)$	There is one solution, l_3 linkage is longer, mechanism contains whole rotation motion pair, and the solution is a double ring	$\sigma^2{}_4(5,6,8)$	$\sigma^3{}_2$ and $\sigma^3{}_3$ worked as the transition boundary that satisfies the link length relationship $l_1 + l_2 = l_3 + l_4$
5	(1/2,0,1/2,0)	$\sigma^3{}_4(4,5,6,8)$	There is one solution, l_3 linkage is longer, mechanism without a revolving pair, and the solution is a single ring	$\sigma^2{}_5(4,5,8)$	$\sigma^3{}_3$ and $\sigma^3{}_4$ worked as the transition boundary that satisfies the link length relationship $l_1 + l_4 = l_2 + l_3$
6	(1/4,1/4,1/2,0)	$\sigma^3{}_5(2,4,5,6)$	No solution, the length of l_3 is longer than the sum of the rest members, and cannot form closed links	$\sigma^2{}_6(5,7,8)$	$\sigma^3{}_1$ and $\sigma^3{}_4$ worked as the transition boundary that satisfies the link length relationship $l_1 + l_2 = l_3 + l_4$
7	(1/2,0,1/4,1/4)				
8	(1/4, 1/4,1/4,1/4)				

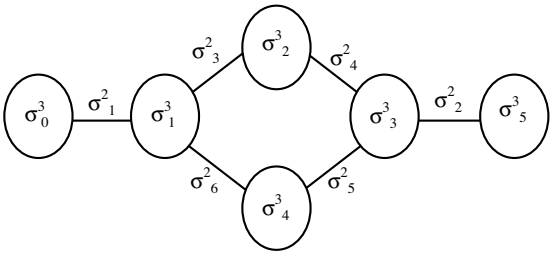


Fig. 5. Evolution relation of type of single ring (l_1, l_2, l_3, l_4).

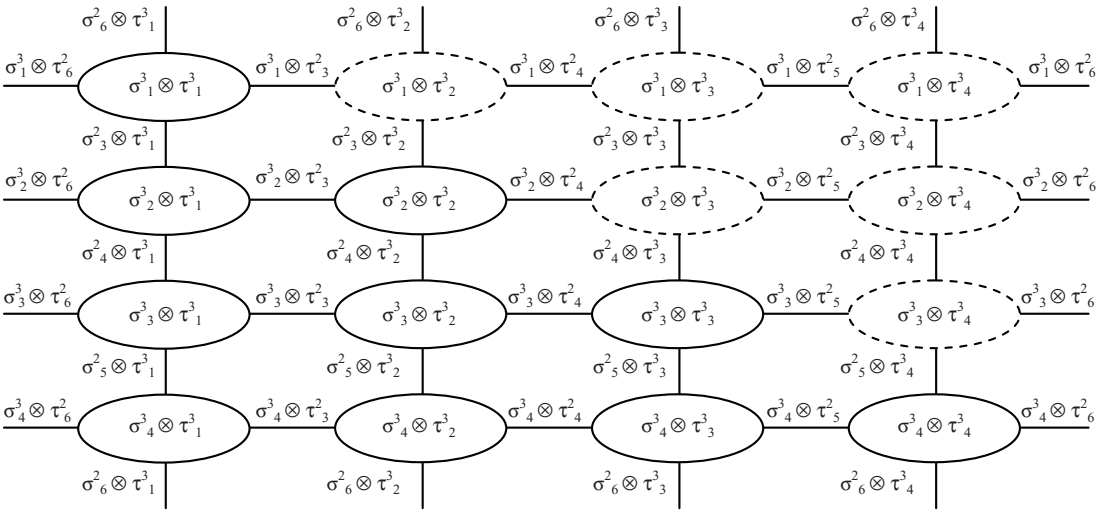


Fig. 6. Results of global scale analysis of first class mechanism.

Single ring (l_1, l_2, l_3, l_4) 4-bar mechanism is divided with the global scale to generate the evolution relationship of the three-dimensional simplex and transition surface, which is shown in Fig. 5. In it, σ_j^i represents the j division area in the i dimension unit. The two dimensions represent the effective transition surface formed by four conditions of Eq. (7). The three dimensions represent the six tetrahedrons in Fig. 4(c) formed by four effective transition planes. The evolution relationship reflects the global distribution characteristics of the motion performance of the single ring (l_1, l_2, l_3, l_4) 4-bar linkage and its evolution rule with the change of bar scale.

The division method, partition condition, and symmetry of the other ring (l_3', l_4', l_5, l_6) are the same as the ring (l_1, l_2, l_3, l_4); so the division result is also the same. In order to distinguish, the division symbol is unified by τ_j^i, and the meaning of the superscript and the subscript is the same.

5.2. The result of double-ring mechanism division

Because of the special double-ring characteristics, the analysis of the whole mechanism can be decomposed into two direct products of single ring analysis results: single ring (l_1, l_2, l_3, l_4) four mechanisms scale types are divided into six types $\sigma^3{}_0 - \sigma^3{}_5$, and single ring ($l_3'$, l_4', l_5, l_6) four mechanisms scale types are divided into six types $\tau^3{}_0 - \tau^3{}_5$. There are $6 \times 6 = 36$ types of direct product of both, writing $\sigma^3{}_i \otimes \tau^3{}_j$ for each type.

The evolutionary relationship between them is shown in Fig. 6; since the types of subscript 0 and 5 are all ineffective types of incapable closed mechanisms, only $4 \times 4 = 16$ types and their evolutionary relationship are given. If the subscript is 1 and 3, the type of direct product will be invalid, because the two rings are equally right and have permutation symmetry. $\sigma^3{}_i \otimes \tau^3{}_j$ and $\sigma^3{}_j \otimes \tau^3{}_i$ have the same properties, and so the actual types are $4 + 3 + 2 + 1 = 10$ types; these ten types are represented by solid line, such as in Fig. 6, and the dotted line represents the type that is symmetrical along the diagonal.

https://doi.org/10.1017/S0263574719000742 Published online by Cambridge University Press

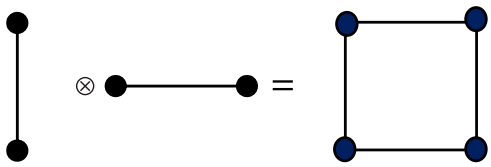


Fig. 7. Geometric meaning of direct product.

In Fig. 6, we take the direct product ${\sigma^3}_1 \otimes {\tau^2}_3$ of transition surface as an example to illustrate the analysis results. According to Table I we get ${\sigma^3}_1$<3, 5, 7, 8>, and its centroid coordinate is (l_1 = 7/16, l_2 = 3/16, l_3 = 4/16, l_4 = 2/16). It satisfies the sum of the longest bar (l_1) and the shortest bar (l_4) is larger than the sum of the other two bars (l_2, l_3), so the first ring has no revolving pair. The other points in ${\sigma^3}_1$ are the same as the nature of the centroid, and it is a monotone transformation. The analysis of the centroid represents the analysis of the mechanism characteristics of all the points in the tetrahedron ${\sigma^3}_1$. Now it's time to analyze τ_3^2. According to the condition of the same weight coefficients of the two rings, τ_3^2 has the same value with σ_3^2 < 3, 5, 8 >. The coordinate of its corresponding centroid is ($l_3' = 5/12$, $l_4' = 3/12$, $l5 = 3/12$, $l6 = 1/12$) which satisfies an equal relationship $l_3' + l6 =_4' + l5$.

Now to analyze ${\tau^2}_3$, according to the two ring with coequal conditions, ${\tau^2}_3$ is the same as ${\sigma^2}_3$<3, 5, 8>, just to make a distinction between the letters, the coordinate of its corresponding centroid is (l_3' = 5/12, l_4' = 3/12, l_5 = 3/12, l_6 = 1/12), satisfy an equal relationship $l_3' + l_6 = l_4' + l_5$. All the combinations in this direct product ${\sigma^3}_1 \otimes {\tau^2}_3$ can meet the collinear condition of the Fig. 3(a) configuration (l_3', l_4', l_5, l_6); the angle of l_3' and l_4' equals zero, and so this transition is a real transition. The analysis procedure of other direct products is similar.

The results of the global scale analysis of the second types of mechanisms are basically the same as those of the first one. The results of the analysis are similar to Fig. 6, but they are only different on the real transition surface.

5.3. Discussion on the direct product of mono form

The direct product of one-dimensional line segment and one-dimensional line segment get a two-dimensional rectangular surface. The boundary of the line segment 1 is x_1 and x_2, the boundary of the line segment 2 is y_1 and y_2, and the four vertex coordinates of a rectangle are $p_1(x_1, y_1)$, $p_2(x_1, y_2)$, $p_3(x_2, y_1)$, $p_4(x_2, y_2)$. The rectangular boundary is composed of two parts: one part is the boundary of the line segment 1 and the direct product of the line segment 2; and the other part is the boundary of the line segment 2 and the direct product of the line segment 1, 1 * 2 + 2 * 1 = 4, as shown in Fig. 7.

The direct product of one-dimensional line segment and two-dimensional triangle is a triangular prism, the number of vertices is 2 * 3 = 6, and the boundary is made up of 1 * 2 triangles and 1 * 3 quadrangles. Four-dimensional complex is obtained by the direct product of two-dimensional triangle and two-dimensional triangle, the number of vertices is 3 * 3 = 9, and the boundary is made up of six three-dimensional three prisms.

The six-dimensional geometry obtained in this paper is the direct product of tetrahedron and tetrahedron. The transition boundary is the direct product of tetrahedron and triangle. Although the geometry of more than four dimensions is difficult to express, the direct product operation provides the vertices and boundaries of the geometric figures after the results of the calculation.

5.4. Virtual prototype simulation experiment

According to the results of global scale analysis of first class mechanism, as shown in Fig. 6, select the linkage length to meet condition ${\sigma^3}_2 \otimes {\tau^3}_1$. Simulation of 6-bar dual ring ABLM is shown in Fig. 8, and its corresponding relation and parameters for each segment are shown in Table II. The elastic buffer mechanism is added as shown in Fig. 9(h). The simulation results of biped fast running and jumping validate the advantages of the ABLM, such as simple control (single motor continuous drive), fast speed (30 km/h), and high jump (twice of the leg length), as shown in Fig. 9(a)–(g). The simulation of quadruped robot also validates this kind of performance, as shown in Fig. 10. The virtual prototype simulation software is ADAMS2015.

https://doi.org/10.1017/S0263574719000742 Published online by Cambridge University Press

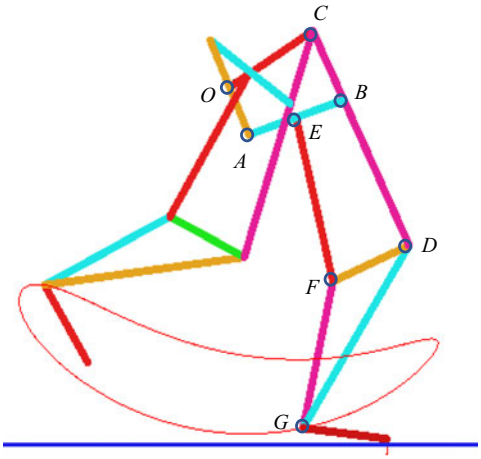


Fig. 8. Simulation of 6-bar dual ring ABLM (single DOF).

Table II. Simulation parameters of each segment.

Number	Segment	Length (mm)	Remarks
1	OA	160	Crank
2	OC	300	Frame
3	AB	350	
4	AE	160	
5	CD	850	
6	EF	550	
7	FG	540	
8	DF	300	
9	DG	930	

6. Theoretical Verification

6.1. Analysis of 3-bar Linkage (Triangle)

Although the 3-bar is connected only to a rigid triangle, it does not constitute a mechanical mechanism. It is the simplest and important for understanding this method.

According to the symmetry property, the partition of triangular structure parameter space can be simplified as a division of unit sphere, as shown in Fig. 11(a). Four independent mutation conditions divide the sphere into six spherical quadrilateral and eight spherical triangles. In the spherical triangle region, the longest edge is smaller than the sum of the other sides, and the solution space is two isolated points. They correspond to two kinds of triangle in different order. Symmetric property can transform these spherical quadrilateral and triangle into one another.

Symmetry can simplify the division into only the first quadrant of the sphere. The division of the first quadrant spherical triangle $<ABC>$ is further simplified to the division of the plane triangle $<ABC>$, as shown in Fig. 11(b).

The plane triangle is divided into four triangles under three mutation conditions over the first quadrant, and the inner solution space of the triangle $<ABC>$ is two isolated points. The other three triangles are empty sets, and the three triangles can be transformed into each other under symmetry permutation group transformation.

Considering the symmetry property, the partition can be simplified to the triangle $<bdC>$ partition, which can be divided into two triangles by a sudden change condition. The inner solution space of the triangle $<bde>$ is two isolated points, and the solution space of the triangle $<beC>$ is an empty set. In addition, point $<d>$ corresponds to equilateral triangle, lines $<db>$ and $<de>$ correspond to two types of isosceles triangle, and line $<be>$ corresponds to the boundary of triangle.

The solution space of a triangle is an isolated point, and there is no need for further division.

https://doi.org/10.1017/S0263574719000742 Published online by Cambridge University Press

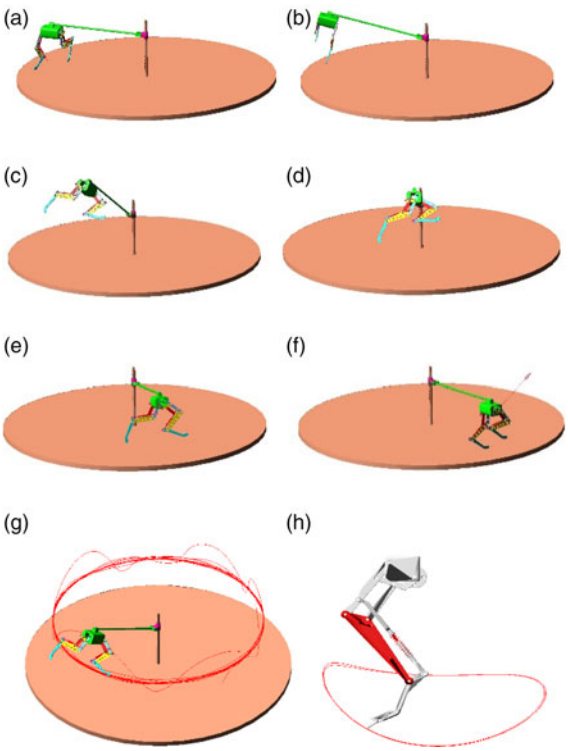


Fig. 9. Biped fast running and jumping simulation (single DOF). (a)–(f) Fast running simulation of 6-bar dual ring ABLM. (g) Jumping simulation of 6-bar dual ring ABLM. (h) Foot track simulation of 6-bar dual ring ABLM.

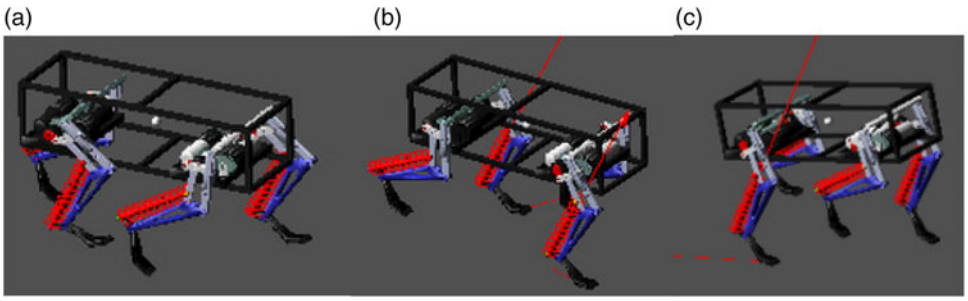


Fig. 10. The simulation of quadruped robot. (a)–(c) Fast running simulation of quadruped robot with 6-bar dual ring ABLM.

6.2. Verified with "Grashof Criterion"

In order to verify the correctness of the GSAM of ABLM proposed in this paper, the method is compared with the "Grashof criterion." The "Grashof criterion" carries out the classical global scale analysis of 4-bar linkage by simple inequality condition.

This method is used to divide the structure space of 4-bar linkage mechanism, and the result contains 3 tetrahedrons, 10 triangles, 12 line segments, and 6 fixed points. As shown in Fig. 12, the conclusion has the following conclusions:

(1) The basic area is a three-dimensional unit (tetrahedron) <1, 2, 4, 6>, which is divided into ${\sigma^3}_0$<1, 2, 3, 6>, ${\sigma^3}_1$<2, 3, 5, 6>, and ${\sigma^3}_2$<2, 3, 4, 6> by the two partition conditions, $l_1-l_2-l_3-l_4= 0$ and $l_1-l_2-l_3-l_4= 0$. Point in σ_0^3 satisfies $l_1 - l_2 - l_3 - l_4 > 0$. The longest bar is longer than the sum of the lengths of the other bars. So, these bars cannot constitute the 4-bar mechanism and the solution space is empty. Point in ${\sigma^3}_1$ satisfies $l_1-l_2-l_3-l_4 > 0$, that is, the sum of the length of the longest bar and the shortest bar is longer than the sum of the lengths of the other two bars. For the 4-bar linkage without the entire turning angle, the solution space

https://doi.org/10.1017/S0263574719000742 Published online by Cambridge University Press

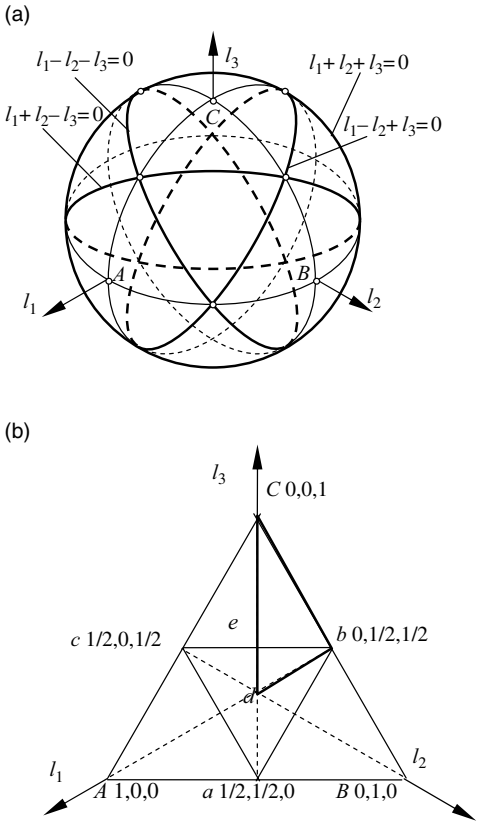


Fig. 11. Space division of structural parameters for three-bar linkage. (a) Division of unit sphere. (b) Division of the plane triangle $<ABC>$.

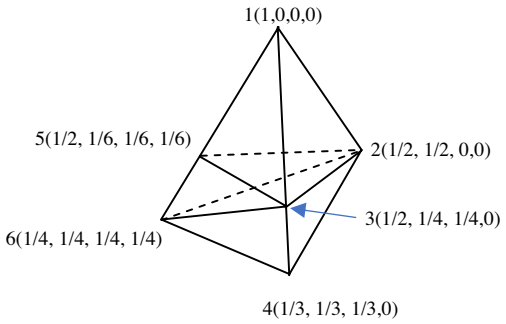


Fig. 12. The analysis area of the 4-bar structure space.

topology is a single circle. Point in ${\sigma^3}_2$ satisfies $l_1-l_2-l_3+l_4<0$, that is, the sum of the length of the longest rod and the shortest bar is less than the sum of the lengths of the other two rods, and the 4-bar linkage with the entire turning angle is the double circle of the solution space. ${\sigma^3}_1$ and ${\sigma^3}_2$ are two basic types of 4-bar mechanism, which is exactly the same with "Grashof criterion."

(2) In 10 two-dimensional units (triangles), ${\sigma^2}_1<2, 3, 5>$ is the boundary of the existence of a 4-bar mechanism. ${\sigma^2}_2<2, 3, 6>$ is the transition boundary between ${\sigma^3}_1$ and ${\sigma^3}_2$, and they correspond to the transition types of two kinds of 4-bar linkage respectively. The division of other two-dimensional units corresponds to the classification of triangles (similar to the analysis process).

(3) In the twelve lines segment, the segment $<2, 6>$ is the mechanism to meet the shortest bar $l_1=l_2$, and meanwhile $l_3=l_4$. Parallel quadrilateral bodies belong to such institutions. Among the six vertices, the vertex $<2>$ satisfies the $l_3=l_4=0$, the infinitesimal neighborhood corresponds to a four bar linkage with a mobile pair, and l_1 and l_2 tend to be infinitely large. Because ${\sigma^3}_0$, ${\sigma^3}_1$ and ${\sigma^3}_2$ all contain vertex $<2>$, so there are three kinds of institutions.

https://doi.org/10.1017/S0263574719000742 Published online by Cambridge University Press

From the above analysis, the analysis of the method to the 4-bar mechanism not only contains the "Grashof criterion," but also analyses some special cases, which is more global.

More importantly, this method solves the important problem of "Grashof criterion," which cannot be used for global scale analysis of arbitrary planar elements.

7. Conclusion

(1) In view of the characteristics of ABLM, a GSAM for mechanism motion performance is proposed, and a system analysis is carried out with a 6-bar ABLM as an example. The 6-bar ABLM designed by this theory is verified by virtual prototype simulation experiment. The simulation results of biped fast running and jumping validate the advantages of the ABLM, such as simple control (single motor continuous drive), fast speed (30 km/h), and high jump (twice of the leg length).

(2) This method is helpful for us to grasp the evolution rule of mechanism performance characteristics as a whole and expand the mind of analysis and synthesis of ABLM. This method also provides a new set of theoretical analysis methods for enriching the innovative design and global scale analysis of ABLM.

(3) The correctness of the method is verified by analyzing the global scale of the 4-bar linkage with the classic "Grashof criterion." Through the analysis of single ring 4-bar and double-ring 6-bar mechanism, it also shows that the GSAM is universal and adapts to the global scale analysis of the ABLM with any single or multi-ring connecting rod. The method has a rigorous mathematical foundation, which provides a theoretical basis for computer programming to achieve global appropriate analysis of planar arbitrary linkage mechanism.

Acknowledgment

This work was supported by the National Natural Science Foundation of China (grant no. 51375410).

References

1. M. P. Murphy, A. Saunders and C. Moreira, "The Little Dog robot," *Int. J. Robotics Res.* **30**, 145–149 (2011).
2. C. Semini, *HyQ—Design and Development of a Hydraulically Actuated Quadruped Robot*, (Italian Institute of Technology, Genova, Italy, 2010).
3. C. Semini, N. G. Tsagarakis, E. Guglielmino, M. Focchi, F. Cannella and D. G. Caldwell, "Design of HyQ a hydraulically and electrically actuated quadruped robot," *Proc. Inst. Mech. Eng. Part I J. Syst. Control Eng.* **6**, 831–849 (2011).
4. J. Zhang, F. Gao, X. Han, X. Chen and X. Han, "Trot gait design and CPG method for a quadruped robot," *J. Bionic Eng.* **11**, 18–25 (2014).
5. M. Li, Z. Jiang, P. Wang, L. Sun and S. S. Ge, "Control of quadruped robot with bionic springy legs in trotting gait," *J. Bionic Eng.* **11**, 188–198 (2014).
6. D. Wooden, M. Malchano and K. Blankespoor, "Autonomous Navigation for BigDog," *IEEE International Conference on Robotics and Automation*, Anchorage, Alaska, USA (2010) pp. 4736–4741.
7. M. Raibert, K. Blankespoor, G. Nelson and R. Playter, "BigDog the Rough-Terrain Quadruped Robot," *Proceedings of the 17th World Congress, the International Federation of Automatic Control*, Seoul, Korea (2008).
8. H. Nie, R. Sun, C. Guo, G. Qin and H. Yu, "Innovative design and performance evaluation of a high-speed bionic mechanical leg," *J. Bionic Eng.* **12**, 352–360 (2015).
9. J. H. Dong, O. S. Sang, J. Lee and S. Kim, "High speed trot-running: Implementation of a hierarchical controller using proprioceptive impedance control on the MIT Cheetah," *Int. J. Robot. Res.* **33**, 1417–1445 (2014).
10. W. Guo, C. Cai, M. Li, F. Zha, P. Wang and K. Wang, "A parallel actuated pantograph leg for high-speed locomotion," *J. Bionic Eng.* **14**, 202–217 (2017).
11. Z. Zhang, D. Chen, K. Chen and H. Chen, "Analysis and comparison of two jumping leg models for bioinspired locust robot," *J. Bionic Eng.*, **13**, 558–571 (2016).
12. J. Zhang, G. Song, Y. Li, G. Qiao, A. Song and A. Wang, "A bio-inspired jumping robot: Modeling, simulation, design, and experimental results," *Mechatronics* **23**, 1123–1140 (2013).
13. Q.-V. Nguyen and H. C. Park, "Design and demonstration of a locust-like jumping mechanism for small-scale robots," *J. Bionic Eng.* **9**, 271–281 (2012).
14. F. Li, W. Liu, X. Fu, G. Bonsignori, U. Scarfogliero, C. Stefanini and P. Dario, "Jumping like an insect: Design and dynamic optimization of a jumping mini robot based on bio-mimetic inspiration," *Mechatronics* **22**, 167–176 (2012).
15. D. W. Haldane, M. M. Plecnik, J. K. Yim and R. S. Fearing, "Robotic vertical jumping agility via series-elastic power modulation," *Sci. Robot.* **1**, eaag2048 (2016).

https://doi.org/10.1017/S0263574719000742 Published online by Cambridge University Press

16. J. Park, K.-S. Kim and S. Kim, "Design of a cat-inspired robotic leg for fast running," *Adv. Robot.* **28**(23), 1587–1598 (2014).
17. S. Seok, A. Wang, M. Y. Chuah, D. Otten, J. Lang and S. Kim, "Design Principles for Highly Efficient Quadrupeds and Implementation on the MIT Cheetah Robot," *IEEE International Conference on Robotics and Automation (ICRA)*, Karlsruhe, Germany, (2013) pp. 6–10.
18. S. Seok, A. Wang, M. Y. Chuah, D. J. Hyun, J. Lee, D. M. Otten, J. H. Lang and S. Kim, "Design principles for energy-efficient legged locomotion and implementation on the MIT Cheetah robot," *IEEE/ASME Trans. Mechatron.* **20**, 1–13 (2014).
19. S. Seok, A. Wang, M. Y. M. Chuah, D. J. Hyun, J. Lee, D. M. Otten, J. H. Lang and S. Kim, "Design principles for energy-efficient legged locomotion and implementation on the MIT cheetah robot," *IEEE/ASME Trans. Mechatron.* **20**, 1117–1129 (2015).
20. The Planar Elliptical Runner, A Clever Two-Legged Robot That Can Run 12 mph on a Treadmill. [G/OL].[2017-05-02]. https://laughingsquid.com/planar-elliptical-runner-two-legged-robot-can-run- treadmill/
21. Handle Legs and Wheels: The best of Both Worlds[G/OL].[2017-02-07]. https://www.bostondynamics.com/handle
22. J. Lei, F. Wang, H. Yu, T. Wang and P. Yuan, "Energy efficiency analysis of quadruped robot with trot gait and combined cycloid foot trajectory," *Chin. J. Mech. Eng.* **27**(1), 138–145 (2014).
23. X. Tian, F. Gao, X. Chen and C. Qi, "Mechanism design and comparison for quadruped robot with parallel-serial leg," *J. Mech. Eng.* **49**(6), 81–88 (2013).
24. M. Li, Z. Jiang and W. Guo, "Single leg system of quadruped bionic robot," *Robot* **36**(1), 21–28 (2014).
25. Y. B. Li, B. Bin, X. W. Rong and J. Meng, "Mechanical design and gait planning of a hydraulically actuated quadruped bionic robot," *J. Shandong Univ.* **41**(5), 32–36 (2011).
26. C. Hui, M. Jian and R. Xuewen, "Design and implementation of high-performance hydraulic drive of quadruped robot SCalf," *Robot* **36**(4), 385–391 (2014).
27. Agility Robotics Introduces Cassie, a Dynamic and Talented Robot Delivery Ostrich [G/OL].[2017-02-09]. http://spectrum.ieee.org/automaton/robotics/industrial-robots/agility-robotics-introduces-cassie-a-dynamic-and-talented-robot-delivery-ostrich
28. Z. Hongbin and S. Lianguan, "Research and optimization design of mechanism for Theo Jansen Bionic Leg," *Chin. J. Mech. Eng.* **53**(15), 101–109 (2017).
29. J. Zhao, J. Xu, B. Gao, N. Xi, F. J. Cintron, M. W. Mutka and L. Xiao "MSU jumper: A single-motor-actuated miniature steerable jumping robot," *IEEE Trans. Robot.* **29**, 602–614 (2013).
30. M. Noh, S. W. Kim, S. An, J. S. Koh and K. J. Cho, "Flea-inspired catapult mechanism for miniature jumping robots," *IEEE Trans. Robot.* **28**, 1007–1018 (2012).
31. G. Kenneally, A. De and D. E. Koditschek, "Design principles for a family of direct-drive legged robots," *IEEE Robot. Autom. Lett.* **1**, 900–907 (2016).
32. J. M. Duperret, G. D. Kenneally, J. L. Pusey and D. E. Koditschek, "Towards a comparative measure of legged agility," *Exp. Robot.* **109**, 3–16 (2016).
33. K. Hapeshi, "A review of nature-inspired algorithms," *J. Bionic Eng.* **7**, S232–S237 (2010).
34. F. Gao, X. Q. Zhang and Y. S. Zhao, "A physical model of the solution space and the atlas of reachable workspace for 2-DOF parallel planar manipulators," *Mech. Mach. Theory* **31**(2), 173–184 (1996).
35. D. F. Zhao, "Dimension classification method of planar mechanism based on convex hull division," *Chin. J. Mech. Eng.* **45**(4), 100–104 (2009).
36. D. F. Zhao, G. Y. Zeng and Y. B. Lu, "The classification method of spherical single-loop mechanisms," *Mech. Mach. Theory* **51**(5), 46–57 (2012).

https://doi.org/10.1017/S0263574719000742 Published online by Cambridge University Press